Journal of
Materials Chemistry B

Accepted Manuscript

ROYAL SOCIETY OF CHEMISTRY

www.rsc.org/materialsB

Journal of
Materials Chemistry B

Cite this: DOI: 10.1039/c0xx00000x

PAPER

www.rsc.org/xxxxxx

Facile synthesis of hyaluronic acid-modified Fe_3O_4/Au composite nanoparticles for targeted dual mode MR/CT imaging of tumors†

Yong Hu,[a1] Jia Yang,[b1] Ping Wei,[a] Jingchao Li,[a] Ling Ding,[a] Guixiang Zhang,[b]* Xiangyang Shi,[a]* Mingwu Shen[a]*

Received (in XXX, XXX) Xth XXXXXXXXX 20XX, Accepted Xth XXXXXXXXX 20XX
DOI: 10.1039/b000000x

A facile co-precipitation approach to synthesizing hyaluronic acid (HA)-modified Fe_3O_4/Au composite nanoparticles (CNPs) for targeted dual mode tumor magnetic resonance (MR) and computed tomography (CT) imaging is reported. In this work, polyethyleneimine (PEI) was employed as a stabilizer to form gold NPs (PEI-Au NPs). In the presence of the PEI-Au NPs, controlled co-precipitation of Fe(II) and Fe(III) salts was performed, leading to the formation of the Fe_3O_4/Au-PEI CNPs, which were further modified with hyaluronic acid (HA). We show that the formed Fe_3O_4/Au-PEI-HA CNPs are colloidally stable, hemocompatible and cytocompatible in a given concentration range, and have a high affinity to target CD44 receptor-overexpressing cancer cells. Due to the presence of Fe_3O_4 and Au components, the formed Fe_3O_4/Au-PEI-HA CNPs display a high r_2 relaxivity (264.16 $mM^{-1}s^{-1}$) and good X-ray attenuation property, rendering them with an ability to be used as a nanoprobe for targeted dual mode MR/CT imaging of CD44 receptor-overexpressing cancer cells *in vitro* and the xenografted tumor model *in vivo*. The Fe_3O_4/Au-PEI-HA CNPs developed *via* this facile approach may hold great promise to be used as a unique platform for precision imaging of CD44 receptor-overexpressing tumors.

Introduction

The past decade has seen a rapid development in molecular imaging technology, which is helpful to realize early cancer diagnosis with high sensitivity and specificity.[1] The different modalities of molecular imaging include optical,[2, 3] magnetic resonance (MR),[4-7] computed tomography (CT),[8-10] ultrasound,[11-13] and positron emission tomography (PET)[14, 15] imaging. However, each single imaging modality possesses its intrinsic limitations, and none of them can completely provide physiological and pathological information independently.[16] Among them, CT imaging is a high-resolution 3-dimensional (3D) tomography technique with high spatial and density resolution.[17-21] On the other hand, MR imaging is one of the most powerful non-invasive medical imaging technique with good spatial resolution and high sensitivity of soft tissues.[5, 6, 22, 23] Therefore, it is valuable to combine these two different modalities for precision imaging of different diseases.

The advances of nanotechnology have enabled the development of various methods to prepare multifunctional nanomaterials for molecular imaging of cancer.[17] Nowadays, magnetic iron oxide (Fe_3O_4) nanoparticles (NPs) have been generally used as T_2-weighted MR contrast agents because of their ability to shorten the T_2 relaxation time of water protons.[24-27] Meanwhile, gold NPs (AuNPs) have been widely used as contrast agents for CT imaging due to their high X-ray attenuation coefficient.[28-30] With the development of synthetic nanotechnology, various kinds of methods have been used to synthesizing Fe_3O_4/Au CNPs.[31] For instance, Yu *et al.*[32] prepared "dumbbell-like" Fe_3O_4/Au CNPs by decomposing iron pentacarbonyl on the surfaces of AuNPs in the presence of oleic acid and oleylamine. In another study, Bao *et al.*[33] firstly prepared AuNPs and thiol-functionalized Fe_3O_4 NPs, then assembled core/shell Fe_3O_4/Au CNPs by simply linking these two kinds of NPs *via* Au-S bonds. Similarly, Caruntu *et al.*[34] synthesized positively charged Fe_3O_4 NPs and negatively charged AuNPs, then assembled the AuNPs onto the surface of the Fe_3O_4 NPs through electrostatic interaction. However, most of the formed Fe_3O_4/Au CNPs have poor colloidal stability and have not been used as contrast agents for dual mode MR/CT imaging.

In order to improve the colloidal stability of the Fe_3O_4/Au CNPs, polymer-mediated methods have been developed for *in vivo* MR/CT dual mode imaging applications. For example, Cai *et al.*[35] utilized a layer-by-layer self-assembly technique to assemble amine-terminated generation 5 poly (amidoamine) dendrimer-entrapped AuNPs onto the Fe_3O_4 core NPs. In our another work,[36] we employed poly(ethylene glycol)-modified polyethyleneimine (*m*PEG-PEI) as a stabilizer to synthesize PEI-entrapped AuNPs (PEI-Au NPs), followed by synthesis of the Fe_3O_4/Au CNPs *via* a one-pot hydrothermal approach, similar to the protocol used to prepare the PEI-coated Fe_3O_4.[37] These successful experiences inspire us to hypothesize that it is possible to construct Fe_3O_4/Au CNPs *via* a simple co-precipitation route.[22]

For the effective diagnosis of tumors, it is indispensable to modify targeting ligands onto the surface of the imaging agents. For instance, folic acid,[5, 38-41] arginine-glycine-aspartic acid peptide,[23, 42, 43] lactobionic acid,[28, 29] and hyaluronic acid (HA)[6, 44, 45] are commonly used ligands that can be modified onto the surface of NPs for targeted tumor imaging applications. As one of the major components of body fluid and vertebrate tissue, HA, not only renders NP-based platform with good colloidal stability and biocompatibility, but also acts as a tumor targeting ligand.[6, 44, 46] In our previous work, we have shown that HA-modified Fe_3O_4 NPs or Fe_3O_4@Au core/shell nanostars can be used for targeted diagnosis or theranostics of CD44 receptor-overexpressing cancer cells.[6, 45] Thus, it is meaningful to immobilize or graft HA onto the surface of Fe_3O_4/Au CNPs for targeted dual mode MR/CT imaging of tumors.

In this research, a facile co-precipitation approach was used to synthesize Fe_3O_4/Au-PEI-HA CNPs for dual mode MR/CT imaging of tumors. PEI was first used as a stabilizer to synthesize PEI-Au NPs *via* sodium borohydride ($NaBH_4$) reduction chemistry. Afterwards, in the presence of the formed PEI-Au NPs, controlled co-precipitation of Fe(II) and Fe(III) salts (molar ratio of Fe(II)/Fe(III) = 1:1.25) was performed to form the Fe_3O_4/Au-PEI CNPs. Finally, the CNPs were modified with HA *via* 1-ethyl-3-[3-dimethylaminopropyl] carbodiimide hydrochloride (EDC) chemistry to obtain the Fe_3O_4/Au-PEI-HA CNPs (Scheme 1). The as-prepared Fe_3O_4/Au-PEI-HA CNPs were characterized *via* different techniques. Their colloidal stability, hemocompatibility, cytocompatibility, specific binding affinity to cancer cells overexpressing CD44 receptors, and dual mode MR/CT imaging of cancer cells *in vitro* and the xenograft tumor model *in vivo* were studied in detail. To our best knowledge, this is the first example related to the fabrication of multifunctional Fe_3O_4/Au-PEI-HA CNPs *via* a facile co-precipitation approach for targeted dual mode MR/CT imaging of tumors.

Experimental

Materials

Sodium hydroxide, ferrous chloride tetrahydrate ($FeCl_2 \cdot 4H_2O$ > 99%), ferric chloride hexahydrate ($FeCl_3 \cdot 6H_2O$ > 99%), and $HAuCl_4 \cdot 4H_2O$ were supplied by Sinopharm Chemical Reagent Co., Ltd (Shanghai, China). $NaBH_4$ and branched PEI (Mw = 25,000) were purchased from Aldrich (St. Louis, MO). HA (Mw = 5,800) was from Zhenjiang Dong Yuan Biotechnology Corporation (Zhenjiang, China). EDC and N-hydroxysuccinimide (NHS) were from J&K Chemical Ltd. (Shanghai, China). All chemicals were used without further purification. HeLa cells (a human cervical carcinoma cell line) were acquired from Institute of Biochemistry and Cell Biology, the Chinese Academy of Sciences (Shanghai, China). Dulbecco's modified eagle medium (DMEM), penicillin, streptomycin, and fetal bovine serum (FBS) were purchased from Hangzhou Jinuo Biomedical Technology (Hangzhou, China). 3-(4,5-Dimethylthiazol-2-yl)-2,5-diphenyltetrazolium bromide (MTT) was from Shanghai Sangon Biological Engineering Technology & Services Co., Ltd. (Shanghai, China). Water used in all experiments was purified using a Milli-Q Plus 185 water purification system (Millipore, Bedford, MA) with a resistivity higher than 18.2 MΩ.cm.

Synthesis of PEI-Au NPs

Branched PEI was used as a template to synthesize AuNPs with the PEI/Au salt molar ratio of 1:100 according to our previous work.[36, 47] Namely, an $HAuCl_4$ aqueous solution (30 mg/mL, 5.4 mL) was added into a PEI aqueous solution (100 mg, 50 mL) under vigorous magnetic stirring. After 30 min, an icy cold $NaBH_4$ solution (45.4 mg, 1.8 mL in water/ethanol, *v/v* = 2:1) was added into the $HAuCl_4$/PEI mixture solution under stirring for 2 h to complete the reaction. The reaction mixture was then purified *via* dialyzing against water (9 times, 2 L) through a dialysis membrane with molecular weight cut-off (MWCO) of 14,000 for 3 days, followed by lyophilization. The prepared PEI-Au NPs were redispersed in 10 mL water and stored at 4 ^oC for further use.

Synthesis of the Fe_3O_4/Au-PEI CNPs

The Fe_3O_4/Au-PEI CNPs were synthesized using a co-precipitation approach. Briefly, 10 mL of $FeCl_2 \cdot 4H_2O$ (89 mg) and $FeCl_3 \cdot 6H_2O$ (157 mg) aqueous solution were mixed with 10 mL of PEI-Au NPs in aqueous solution and the mixture was stirred for 3-5 min to ensure uniform mixing. Afterwards, a sodium hydroxide (1.0 g, 5 mL) aqueous solution was added into the above mixture solution under stirring, and the suspension was continuously stirred for 30 min at 80 ^oC. Then the mixture was cooled down to room temperature, the product (denoted as Fe_3O_4/Au-PEI CNPs) was collected by magnetic separation and purified 5 times with water. Finally, the prepared Fe_3O_4/Au-PEI CNPs were redispersed in water. For comparison, Fe_3O_4-PEI NPs in the absence of the PEI-Au NPs were also prepared in a manner similar to that used to form the Fe_3O_4/Au-PEI CNPs. The only difference is the use of PEI instead of the use of the PEI-Au NPs.

Synthesis of the Fe_3O_4/Au-PEI-HA CNPs

An aqueous HA solution (9 mg, 5 mL) was mixed with 5 mL DMSO containing EDC (2.98 mg) and NHS (1.79 mg) under vigorous magnetic stirring for 3 h to activate the carboxyl group of HA. Then, the activated HA solution was dropwise added into the above aqueous suspension of the Fe_3O_4/Au-PEI CNPs (25 mg, 10 mL) under magnetic stirring for 3 days. The formed multifunctional particles (denoted as Fe_3O_4/Au-PEI-HA CNPs) were washed with water for 4 times and redispersed in 10 mL water.

Characterization techniques

The crystalline structure of the Fe_3O_4/Au-PEI CNPs was analyzed by X-ray diffraction (XRD) at a 2θ range of 5-90°. Step scans were performed using a D/max 2550 PC X-ray diffractometer (Rigaku Cop., Tokyo, Japan) with Cu K radiation (λ = 0.154 nm) at 40 kV and 200 mA. The organic component of the samples was quantified by thermo gravimetric analysis (TGA) using a TG 209 F1 (NETZSCH Instruments Co., Ltd., Selb/Bavaria, Germany) thermogravimetric analyzer. The samples were heated from 25 °C to 700 °C at a rate of 10 °C/min under nitrogen atmosphere. UV-vis spectra were collected by a Lambda 25 UV-vis spectrophotometer (Perkin Elmer, Boston, MA). Zeta potential and hydrodynamic size were measured by a Malvern Zetasizer Nano ZS model ZEN3600 (Worcestershire, U. K.) equipped with a standard 633 nm laser. Samples were

dispersed in water at a particle concentration of 0.1 mg/mL before measurements. The size and morphology of the particles were characterized by TEM (JEOL, Tokyo, Japan) at an operating voltage of 200 kV. TEM samples were prepared by depositing one drop of the diluted particle suspension (5 μL) onto a carbon-coated copper grid and air dried before measurements. The Fe and Au concentrations of the samples were determined by a Leeman Prodigy Inductively Coupled Plasma-Atomic Emission Spectroscopy (ICP-OES) system (Hudson, NH). The samples were dissolved in aqua regia and diluted with water before measurements. T_2 relaxometry of the Fe_3O_4/Au-PEI-HA CNPs at Fe concentrations of 0.0025-0.04 mM was performed using an NMI20-Analyst NMR analyzing and imaging system (Shanghai Niumag Corporation, Shanghai, China). The parameters were set as follows: magnet field = 0.5 T, point resolution = 156 mm ×156 mm, section thickness = 0.6 mm, TR = 6000 ms, TE = 100 ms, and number of excitation = 1. T_2 relaxivity (r_2) was calculated by a linear fitting of the inverse T_2 ($1/T_2$) relaxation time as a function of the Fe concentration. Evaluation of the X-ray attenuation intensity of the Fe_3O_4/Au-PEI-HA CNPs at Au concentrations of 0-16 mM was performed using a GE LightSpeed VCT imaging system (GE Medical Systems, Milwaukee, WI) with 100 kV, 80 mA, and a slice thickness of 0.625 mm. Contrast enhancement was determined in Hounsfield Units (HU) for each sample with a given Au concentration.

Hemolysis assay

Fresh human blood stabilized with heparin was kindly provided by Shanghai General Hospital (Shanghai, China) and used after approval by the Ethical Committee of Shanghai General Hospital. Human red blood cells (HRBCs) were purified according to protocols described in the literature.[5] After that, the suspension of HRBCs was 10 times diluted with PBS, and 0.1 mL of the diluted HRBC suspension was gently mixed with 0.9 mL PBS containing the Fe_3O_4/Au-PEI-HA CNPs at different Fe concentrations (50, 100, 300, and 600 μg/mL, respectively), 0.9 mL water (as positive control), and 0.9 mL PBS (as negative control), respectively. After maintaining still for 2 h at room temperature, the mixtures were centrifuged (10,000 rpm, 1 min), the photograph of the samples was taken, and the absorbance of the supernatants (hemoglobin) was measured by a Perkin Elmer Lambda 25 UV-vis spectrophotometer. The hemolysis percentages of different samples were calculated according to a previously reported method.[48]

Cell culture

HeLa cells overexpressing CD44 receptors[49, 50] were cultured and passaged in 25-cm^2 plates with DMEM supplemented with 10% FBS and 1% penicillin/streptomycin under 37 °C and 5% CO_2. HeLa cells grown in HA-free medium expressed high-level CD44 receptors (denoted as HeLa-HCD44), while the cells pre-treated with HA-containing medium (2 mM) for 2 h or longer expressed low-level CD44 receptors (denoted as HeLa-LCD44). Unless otherwise stated, the term of HeLa cells always represents the HeLa-HCD44 cells.

Cytotoxicity assay and cell morphology observation

In vitro cytotoxicity of the Fe_3O_4/Au-PEI-HA CNPs was evaluated by MTT viability assay of HeLa cells according to protocols described in the literature.[5, 6] Briefly, HeLa cells were seeded into a 96-well plate at a density of 1×10^4 cells/well with 200 μL of fresh DMEM. After incubation at 37 °C and 5% CO_2 overnight to bring the cells to confluence, the medium was replaced with 200 μL fresh medium containing PBS (control) or Fe_3O_4/Au-PEI-HA CNPs with different Fe concentrations (0.2, 0.4, 0.8, 1.5, and 2.0 mM, respectively). The cells were incubated for 24 h at 37 °C and 5% CO_2. Thereafter, MTT (20 μL in PBS, 5 mg/mL) was added to each well and the cells were incubated continuously for an additional 4 h. After that, the medium was carefully removed, and DMSO (150 μL) was added to dissolve the insoluble formazan crystals. The absorbance at 570 nm in each well was recorded using a Thermo Scientific Multiskan MK3 ELISA reader (Thermo Scientific, Hudson, NH). Mean and standard deviation (SD) of 5 parallel wells were reported for each sample.

To further confirm the cytotoxicity of the Fe_3O_4/Au-PEI-HA CNPs, after treatment with PBS or the Fe_3O_4/Au-PEI-HA CNPs at different Fe concentrations (0.2, 0.4, 0.8, 1.5, and 2.0 mM, respectively) for 24 h, the cell morphology was observed using a Leica DM IL LED inverted phase contrast microscope with a magnification of 200 × for each sample.

***In vitro* cellular uptake assay**

ICP-OES was carried out to investigate the cellular uptake of the Fe_3O_4/Au-PEI-HA CNPs by HeLa-HCD44 or HeLa-LCD44 cells. Both kinds of cells were seeded into 12-well plates at a density of 2×10^5 cells/well. After incubation at 37 °C and 5% CO_2 overnight, the medium was replaced with fresh medium containing the Fe_3O_4/Au-PEI-HA CNPs at different Fe concentrations (0.2, 0.4 and 0.6 mM, respectively). After 4 h incubation, the medium was discarded carefully and the cells were washed with PBS for 5 times, trypsinized, centrifuged, and counted by Handheld Automated Cell Counter (Millipore, Billerica, MA). The remaining cells were lysed using an aqua regia solution (1.0 mL) for 2 days, and then the Au uptake in the cells was quantified by ICP-OES.

Prussian blue staining assay

Prussian blue staining of HeLa-HCD44 or HeLa-LCD44 cells was performed to qualitatively confirm the cellular Fe uptake. Both kinds of cells were seeded in 12-well plates at a density of 2×10^5 cells/well. After incubation at 37 °C and 5% CO_2 overnight to bring the cells to confluence, the medium was replaced with fresh medium containing the Fe_3O_4/Au-PEI-HA CNPs at different Fe concentrations (0.2, 0.4, and 0.6 mM, respectively) and the cells were incubated for another 4 h. Then, the cells were washed for 3 times with PBS, fixed with glutaraldehyde solution (2.5%) at 4 °C for 15 min, and stained with Prussian blue reagent (Beijing Leagene Biotechnology Co., Ltd., Beijing, China. Perls stain A1 and Perls stain A2 was mixed equivalently.) at 37 °C for 30 min.[37] The cells were then imaged by Leica DM IL LED inverted phase contrast microscope with a magnification of 200 × for each sample

***In vitro* MR/CT imaging of cancer cells**

In vitro MR and CT imaging of cancer cells was performed according to the literature.[45] In brief, HeLa-HCD44 or HeLa-

LCD44 cells were seeded into 6-well plates at a density of 2 × 10^6 cells/well with 2 mL of fresh DMEM and incubated at 37 °C and 5% CO_2 overnight to bring the cells to confluence. Then the medium was replaced with fresh medium containing Fe_3O_4/Au-PEI-HA CNPs at different Fe concentrations (0.1, 0.2, 0.4, and 0.6 mM, respectively) and the cells were incubated at 37 °C and 5% CO_2 for 6 h. Afterwards, the cells were washed 5 times with PBS, trypsinized, centrifuged, and resuspended in 1 mL PBS (containing 0.5% agarose). T_2-weighted MR imaging of each sample was carried out using a 1.5 T Signa HDxt superconductor clinical MR system (GE Medical Systems, Milwaukee, WI) under the following conditions: point resolution = 156 mm × 156 mm, section thickness = 0.6 mm, TR = 3000 ms, TE = 90.7 ms, and number of excitation = 1. The cell samples for CT imaging were prepared similar to the protocol described above. Instead of the use of Fe concentrations of the Fe_3O_4/Au-PEI-HA CNPs, we used Au concentrations (0.125, 0.25, 0.5, and 1.0 mM, respectively) of the particles as a measure. CT image of each sample was collected using GE LightSpeed VCT imaging system with 100 kV, 80 mA, and a slice thickness of 0.625 mm.

In vivo MR/CT imaging of a xenografted tumor model

All animal experiments were approved by institutional committee for animal care and also carried out in agreement with the policies of the National Ministry of Health. Male 4- to 6-week-old BALB/c nude mice (15-20 g) were purchased from Shanghai Slac Laboratory Animal Center (Shanghai, China). To establish the xenografted tumor model, HeLa cells (2 × 10^6/mouse) were implanted subcutaneously into the back of the nude mice. When the tumor nodules reached 0.5-0.8 cm in diameter (3 weeks postinjection), the mice were anesthetized by intraperitoneal injection of pentobarbital sodium (40 mg/kg) and divided into 3 groups: For Group 1, the mice were injected with the Fe_3O_4/Au-PEI-HA CNPs; Group 2, the mice were pre-injected with free HA (1 mM, 0.1 mL PBS) for 1 h and then injected with the particle solution; and Group 3, the mice were injected with the mixture of free HA (1 mM, 0.1 mL PBS) and Fe_3O_4/Au-PEI-HA CNPs. In all cases, the dose of the Fe_3O_4/Au-PEI-HA CNPs ([Fe] = 215.29 mM, [Au] = 50 mM, 0.1 mL PBS) was consistent and all mice were intravenously injected through the tail vein.

For T_2-weighted MR imaging, each mouse was imaged using a 1.5 T Signa HDxt superconductor clinical MR system coupled with a custom-built rodent receiver coil (Chenguang Med Tech, Shanghai, China). Two-dimensional (2D) spin-echo MR images were obtained before and at the time points of 0.5, 1, 2, 4, and 6 h postinjection of the Fe_3O_4/Au-PEI-HA CNPs with the conditions similar to those used for *in vitro* MR imaging of cancer cells. For CT imaging, each mouse was imaged using a GE LightSpeed VCT imaging system with the parameters similar to those used for *in vitro* CT imaging of cancer cells.

In vivo biodistribution

To assess the biodistribution of the Fe_3O_4/Au-PEI-HA CNPs, the tumor-bearing BALB/c nude mice were first anesthetized by intraperitoneal injection of pentobarbital sodium (40 mg/kg). Then, after intravenous injection of the Fe_3O_4/Au-PEI-HA CNPs ([Fe] = 215.29 mM, [Au] = 50 mM, 0.1 mL PBS for each mouse) *via* the tail vein, the mice were sacrificed at 2, 4, 8, 12, and 24 h postinjection (n = 1 at each time point) and the heart, liver, spleen, lung, kidney, and tumor were harvested, weighed and digested by aqua regia for 2 days. The tumor-bearing mice before treatment were used as control, and the Fe or Au content in the organs was simultaneously determined by ICP-OES.

Histological examinations

All tumor-bearing mice were injected with the Fe_3O_4/Au-PEI-HA CNPs ([Fe] = 215.29 mM, [Au] = 50 mM, 0.1 mL PBS) *via* the tail vein. After 15 days, the major organs of mice including heart, liver, spleen, lung, kidney and tumor were extracted, fixed in formaldehyde, embedded in paraffin, sectioned, dewaxed, and stained with hematoxylin and eosin (H&E) according to our previous work.[38] Finally, the histological sections were observed under a phase contrast microscope with a magnification of 200 × for each sample.

Statistical analysis

One-way ANOVA statistical analysis was performed to evaluate the significance of the experimental data. 0.05 was selected as the significance level, and the data were indicated with (*) for $p < 0.05$, (**) for $p < 0.01$, and (***) for $p < 0.001$, respectively.

Results and discussion

Synthesis and characterization of the Fe_3O_4/Au-PEI-HA CNPs

According to our previous work,[36, 51] PEI-Au NPs (PEI/Au salt molar ratio of 1:100) were first prepared by a common $NaBH_4$ reduction route. In the presence of the PEI-Au NPs, controlled co-precipitation of Fe(II) and Fe(III) salts led to the formation of the Fe_3O_4/Au-PEI CNPs, which were subsequently grafted with HA *via* EDC coupling (Scheme 1).

PEI was used as a stabilizer to synthesize PEI-Au NPs *via* $NaBH_4$ reduction chemistry and their size and morphology were characterized by TEM (Fig. S1, ESI†). We can see that the formed PEI-Au NPs have a spherical shape and are relatively uniform with a mean diameter of 3.0 ± 0.5 nm. The PEI-Au NPs were then used as a stabilizer to prepare Fe_3O_4/Au-PEI CNPs *via* a co-precipitation route. UV-vis spectroscopy was used to characterize the products (Fig. 1a). Fe_3O_4/Au-PEI CNPs display a surface plasmon resonance (SPR) peak at 545 nm, while the Fe_3O_4-PEI NPs synthesized using PEI as a stabilizer under similar conditions do not exhibit such a peak in the same region, suggesting the presence of AuNPs in the CNPs. The crystal structure of the formed Fe_3O_4/Au-PEI CNPs was then characterized by XRD (Fig. 1b). It can be seen that the XRD pattern of the CNPs at 30.2, 35.4, 43.2, 53.4, 57.0, 62.7° well matches the [220], [311], [400], [422], [511], [440] planes of the Fe_3O_4 crystals, and that at 38.1, 44.2, 64.7, 77.7, 81.8° matches the [111], [200], [220], [311], [222] planes of the Au crystals, respectively. The XRD results suggest the presence of both Fe_3O_4 and Au crystals in the as-formed Fe_3O_4/Au-PEI CNPs.

Next, HA was grafted onto the surface of the Fe_3O_4/Au-PEI CNPs *via* EDC coupling to afford the particles with improved biocompatibility and targeting specificity. It should be noted that the higher Mw of HA usually renders the HA-modified NPs with higher targeting specificity to CD44 receptor-expressing cancer cells.[6, 52] However, the higher Mw free HA is quite viscous in

solution, which is not suitable for the designed experiments to block the CD44 receptors *in vitro* and *in vivo*. Thus, the HA with an intermediate Mw of 5,800 was chosen to be conjugated on the surface of the Fe_3O_4/Au-PEI CNPs. TGA was carried out to analyze the composition of product (Fig. S2, ESI†). For the Fe_3O_4/Au-PEI CNPs, due to the removal of free water and hydrate water below 150 ^oC as well as the degradation of PEI at the same temperature, the final weight loss was estimated to be about 4.7%, indicating the successful coating of PEI onto the surface of CNPs (Fig. S2, Curve a, ESI†). After the modification of HA, the Fe_3O_4/Au-PEI-HA CNPs show a weight loss of 6.5% because of the further HA coating and the loading percentage of HA was estimated to be 1.8% (Fig. S2, Curve b, ESI†).

The surface potential of the particles before and after HA modification was characterized (Table 1). It can be clearly seen that the positive surface potential of the Fe_3O_4/Au-PEI CNPs (+36.1 mV) is reversed to be negative after the HA modification to form the Fe_3O_4/Au-PEI-HA CNPs (-19.6 mV), confirming the successful HA grafting. The hydrodynamic size of the CNPs was also analyzed (Table 1). It appears that the HA modification renders the Fe_3O_4/Au-PEI-HA CNPs with larger hydrodynamic size (384.2 nm) than the CNPs before HA modification (339.3 nm). Moreover, DLS was also used to evaluate the colloidal stability of the particles. We show that the hydrodynamic size of the Fe_3O_4/Au-PEI-HA CNPs does not have any obvious changes over a period of 15 days. What's more, after dispersing the Fe_3O_4/Au-PEI-HA CNPs in different media (water, PBS and DMEM), the particles are colloidally stable and no precipitation can be seen over a time period of one month (Fig. S3, ESI†). This suggests that the formed Fe_3O_4/Au-PEI-HA CNPs possess a good colloidal stability.

The morphology and structure of the Fe_3O_4/Au-PEI-HA CNPs were characterized by TEM. The TEM image of the Fe_3O_4/Au-PEI-HA CNPs is not very clear, which could be due to the existence of a large amount of macromolecular coating of PEI and HA on the particle surface. As shown in Fig. 2a, some darkened Au nanocrystals are surrounded on the surface of the Fe_3O_4 NPs with a size around 9.7 nm (Fig. S4, ESI†). The larger Au crystals than the pristine PEI-Au NPs (3.0 nm) is likely due to the further Ostwald ripening process under the co-precipitation conditions. Additionally, the coating of the AuNPs on the surface of the Fe_3O_4 NPs is not uniform, similar to our previous works.[35, 36] Some aggregated or interconnected particles in the TEM image could be ascribed to the TEM sample preparation process, especially the air-drying process of the aqueous suspension.[35] It is important to note that the non-uniform distribution of Au crystals around the surface of the Fe_3O_4 NPs is beneficial for the CNPs to have non-compromised T_2 relaxivity, because the accessibility of water protons does not have appreciable changes when compared to the Fe_3O_4 NPs without Au coating (see below), in agreement with our previous work.[36] The EDS spectrum further confirms the presence of Au and Fe elements in the Fe_3O_4/Au-PEI-HA CNPs (Fig. 2b). The existence of Cu element should be due to the copper grid used for TEM sample preparation.

Furthermore, the Fe_3O_4/Au molar ratio of the Fe_3O_4/Au-PEI-HA CNPs was estimated to be 1:1.01 according to ICP-OES. It's worth noting that the Au content of the particles in this work is much higher than that of CNPs formed *via* a LbL self-assembly approach reported in our previous work,[35] which is important to render the particles with non-compromised CT imaging sensitivity.

MR relaxometry and X-ray attenuation property

The combination of Fe_3O_4 NPs and Au NPs is expected to render the Fe_3O_4/Au-PEI-HA CNPs with both T_2 relaxivity allowing for MR imaging and X-ray attenuation property amenable for CT imaging, respectively. We explored the T_2 relaxometry of the CNPs (Fig. 3a). The MR signal intensity decreases with the Fe concentration. The plot of the T_2 relaxation rate ($1/T_2$) as a function of Fe concentration shows that the $1/T_2$ of the particle suspension increases linearly with the Fe concentration and the T_2 relaxivity (r_2) of the CNPs was calculated to be 264.16 $mM^{-1}s^{-1}$ (Fig. 3b), which is much higher than those of Fe_3O_4 NPs or Fe_3O_4/Au CNPs reported in the literature.[5, 6, 35-37] Our results suggest that the Fe_3O_4/Au-PEI-HA CNPs could be used for T_2-weighted MR imaging applications.

AuNPs have been intensively utilized as CT contrast agents due to their better X-ray attenuation property than iodinated CT contrast agents.[8, 51] It is clear that the X-ray attenuation intensity of the Fe_3O_4/Au-PEI-HA CNPs increases with the increase of Au concentration (Fig. 3c). By plotting the CT value as a function of Au concentration, we show that the CT value of the CNPs increases linearly with the Au concentration (Fig. 3d), implying the potential to use the developed Fe_3O_4/Au-PEI-HA CNPs for CT imaging applications.

Hemolysis assay

For *in vivo* biomedical applications, the hemocompatibility of the probe should be first evaluated. The hemolysis activity of the Fe_3O_4/Au-PEI-HA CNPs was tested (Fig. 4). We show that the Fe_3O_4/Au-PEI-HA CNPs do not induce any obvious hemolysis effect in an Fe concentration range of 50-600 μg/mL when compared with the negative PBS control (bottom right inset of Fig. 4). In contrast, the positive control (water) causes a significant hemolysis effect. Based on the hemoglobin absorbance at 541 nm, the highest hemolysis percentage of the Fe_3O_4/Au-PEI-HA CNPs was calculated to be 0.98% (top right inset of Fig. 4), which is much lower than the threshold value of 5%.[36] Our results indicate that the Fe_3O_4/Au-PEI-HA CNPs have an excellent hemocompatibility in the given concentration range.

Cytotoxicity assay and cell morphology observation

In vitro cytotoxicity of the Fe_3O_4/Au-PEI-HA CNPs was assessed using MTT assay (Fig. 5). Obviously, the Fe_3O_4/Au-PEI-HA CNPs do not shown any apparent cytotoxicity to HeLa cells at different Fe concentrations (0, 0.2, 0.4, 0.8, 1.5, and 2.0 mM, respectively) for 24 h. The cell viability still maintains as high as 80% even at a high Fe concentration of 2.0 mM.

The cytocompatibility of the Fe_3O_4/Au-PEI-HA CNPs was further validated by observing the morphology of HeLa cells treated with the particles at different Fe concentrations for 24 h (Fig. S5, ESI†). It can be seen that the morphology of cells treated with the Fe_3O_4/Au-PEI-HA CNPs in the given concentration range is similar to the control cells treated with PBS. Overall, the results of MTT assay and cell morphology observation clearly suggest that the formed Fe_3O_4/Au-PEI-HA CNPs have a good cytocompatibility in the studied Fe

concentration range.

Cellular uptake

The conjugation of HA is expected to render the formed Fe_3O_4/Au-PEI-HA CNPs with target specificity to CD44 receptor-overexpressing cancer cells. We next quantitatively evaluated the cellular uptake of the Fe_3O_4/Au-PEI-HA CNPs using ICP-OES (Fig. 6). It can be seen that after 4 h incubation with the Fe_3O_4/Au-PEI-HA CNPs, HeLa-HCD44 cells display significantly higher Fe uptake than HeLa-LCD44 cells, which is presumably due to the HA-mediated specific cellular uptake of the particles.

The cellular uptake of the Fe_3O_4/Au-PEI-HA CNPs by HeLa-HCD44 and HeLa-LCD44 cells was further qualitatively validated by Prussian blue staining (Fig. 7). Compared with the cells treated with PBS that do not display the blue staining (Fig. 7a, e), all the other cells treated with the Fe_3O_4/Au-PEI-HA CNPs display blue staining in a concentration-dependent manner (Fig. 7b-d, f-h). Importantly, at the same Fe concentration (0.2, 0.4, and 0.6 mM, respectively), HeLa-HCD44 cells display much more obvious blue staining than HeLa-LCD44 cells, implying the much more enhanced cellular Fe uptake in HeLa-HCD44 cells. This further confirms the targeting role played by HA modified onto the surface of CNPs, in agreement with the literature.[6, 45]

Targeted dual mode MR/CT imaging of cancer cells *in vitro*

With the proven high r_2 relaxivity, good X-ray attenuation property, and targeting specificity of the Fe_3O_4/Au-PEI-HA CNPs to CD44 receptor-overexpressed cancer cells, we next investigated the feasibility to use the Fe_3O_4/Au-PEI-HA CNPs as a nanoprobe for targeted MR/CT dual mode imaging of cancer cells *in vitro*.

MR imaging data (Fig. 8a) reveal that the MR signal intensity of both cells decreases with the increase of Fe concentration. However, the decreasing trend of the HeLa-HCD44 cells is much larger than that of the HeLa-LCD44 cells at the same Fe concentrations. This result was further validated by quantitative analysis of the MR signal intensity of the cells (Fig. 8b), where the MR signal intensity of the HeLa-HCD44 is much lower than that of the HeLa-LCD44 cells under the same Fe concentrations ($p < 0.001$). It's worth noting that the Fe_3O_4/Au-PEI-HA CNPs enhance the cell-to-background MR contrast through cell labeling. We could sensitively detect 2×10^6 cells/mL on the 1.5 T MR imaging system when HeLa cells were incubated with the Fe_3O_4/Au-PEI-HA CNPs at the lowest Fe concentration of 0.1 mM (5.6 μg/mL) for 24 h. This MR detection sensitivity is much higher than that reported by Magnitsky *et al.* (100 cells labeled with Feridex at an Fe concentration of 25 μg/mL).[53]

The Fe_3O_4/Au-PEI-HA CNPs also enabled CT imaging of HeLa cells. Due to the fact that it is difficult to differentiate the brightness difference of the cell samples by eyes in the CT images (Fig. 8c), similar to our previous work,[45] it's essential to quantify the CT values of the cells (Fig. 8d). The CT values of both HeLa-HCD44 and HeLa-LCD44 cells treated with the Fe_3O_4/Au-PEI-HA CNPs are much higher than that of the corresponding cells treated with PBS (control), and the cells treated with the particles with higher Au concentration display higher CT values for both cells. Importantly, the CT values of the HeLa-HCD44 cells are much higher than those of the HeLa-LCD44 cells at same Au concentrations due to the role played by HA-mediated targeting, corroborating the MR imaging data.

Targeted dual mode MR/CT imaging of tumors *in vivo*

We next investigated the potential to use the Fe_3O_4/Au-PEI-HA CNPs as a probe for dual mode MR/CT imaging of a xenografted tumor model. MR imaging data (Fig. 9a) reveal that the MR signal of the tumor site gradually decreases with the time postinjection. The tumor site becomes the darkest at 2 h postinjection likely due to the maximum tumor uptake of the Fe_3O_4/Au-PEI-HA CNPs. At 4 h postinjection, the tumor MR signal gradually recovers due to the further diffusion and tissue metabolization of the particles. However, at each time point, the tumor MR signal of Group 1 is always much lower than that of the other two groups. It seems that preinjection of free HA or co-injection of free HA with the Fe_3O_4/Au-PEI-HA CNPs is able to make the CD44 receptors on the cells surface occupied, leading to significantly decreased uptake of the particles through a receptor-mediated manner. Further quantitative analysis of the tumor MR signal intensity as a function of the time postinjection also demonstrates the same trend of the tumor MR signal intensity changes (Fig. 9b), and shows the statistical significant difference between Group 1 and Group 2 or 3 ($p < 0.01$).

For CT imaging, the tumor site (pointed by the red arrow) is brighter after the injection of the CNPs when compared with that before injection (Fig. 9c). At 4 h postinjection, the tumor CT signal intensity gradually reduces. It is noted that the tumor CT signal of Group 1 is always much higher than that of the other two groups at each time point, and this can be reflected by quantitative analysis of the tumor CT value as a function of the time postinjection (Fig. 9d). Our results show that the developed CNPs are able to induce specific CT imaging of the tumors *via* HA-mediated targeting, corroborating the MR imaging data. Taken together, we can conclude that the developed Fe_3O_4/Au-PEI-HA CNPs are able to be used as a probe for targeted MR/CT dual mode imaging of CD44 receptor-overexpressing tumors.

***In vivo* biodistribution and histological examinations**

The biodistribution of the Fe_3O_4/Au-PEI-HA CNPs by the major organs including heart, liver, spleen, lung, kidney, and tumor were quantified using ICP-OES (Fig. S6, ESI†). It is clear that the Au and Fe concentrations in all the organs of the treated mice is much higher than that of the control mice before injection. The largest accumulation of Fe and Au in the tumor appears at 2 h postinjection of the Fe_3O_4/Au-PEI-HA CNPs, which is in accordance with the data of *in vivo* MR/CT imaging of tumors. It should be pointed out that only a quite small amount of Fe or Au is accumulated in the heart, lung, kidney, and tumor, while the majority uptake of Fe or Au occurs in the liver and spleen at the studied time points. This is likely due to the clearance effect of the reticuloendothelial system (RES).[54, 55] Although detailed pharmacokinetic studies still need to be carried out for a clear understanding of their biodistribution, our preliminary data show that the particles are able to be gradually excreted from the body. This ensures the *in vivo* biocompatibility of the particles.

The assessment of potential tissue toxicity was further carried out by H&E staining of the major organs sections including the heart, liver, spleen, lung, kidney and tumor at 15 days postinjection of the particles (Fig. 10). All organs of the mice

treated with the Fe_3O_4/Au-PEI-HA CNPs display similar cellular structure and morphology when compared to the control group treated with PBS. Our results suggest that the Fe_3O_4/Au-PEI-HA CNPs do not cause any obvious *in vivo* toxicity, thereby holding a great potential to be used for *in vivo* biomedical applications.

Conclusion

In summary, we developed HA-modified Fe_3O_4/Au CNPs for targeted dual mode MR/CT imaging of tumors. In the presence of PEI-Au NPs, controlled co-precipitation of Fe(II) and Fe(III) salts leads to the formation of the Fe_3O_4/Au-PEI CNPs that can be further conjugated with HA through EDC coupling. The developed Fe_3O_4/Au-PEI-HA CNPs display good water dispersibility, colloidal stability, hemocompatibility, and cytocompatibility in the given concentration range. With the relatively high r_2 relaxivity (264.16 $mM^{-1}s^{-1}$), good X-ray attenuation property, and HA-mediated targeting specificity to CD44 receptor-overexpressing cancer cells, the Fe_3O_4/Au-PEI-HA CNPs are able to be used as a probe for targeted dual mode MR/CT imaging of cancer cells *in vitro* and the xenografted tumor model *in vivo*. By incorporating different targeting ligands (e.g., DNA aptamers, peptides, or sugars, etc.) and therapeutic molecules, it is expected that such PEI-stabilized Fe_3O_4/Au CNPs may be developed as a unique platform for diagnosis and therapy of different diseases.

Acknowledgements

This research is financially supported by the National Natural Science Foundation of China (21273032, 81341050, and 81371623), the Sino-German Center for Research Promotion (GZ899), and the Program for Professor of Special Appointment (Eastern Scholar) at Shanghai Institutions of Higher Learning. M. Shen thanks the Fundamental Research Funds for the Central Universities. Y. H. thanks the Innovation Funds of Donghua University Master Dissertation of Excellence (EG2015021).

Notes and references

[a] *College of Chemistry, Chemical Engineering and Biotechnology, Donghua University, Shanghai 201620, People's Republic of China*
E-mail: xshi@dhu.edu.cn (X. Shi), mingwu_shen@yahoo.com (M. Shen)
[b] *Department of Radiology, Shanghai General Hospital, School of Medicine, Shanghai Jiaotong University, Shanghai 200080, People's Republic of China*
E-mail: guixiangzhang@sina.com (G. Zhang)
[1]*Yong Hu and Jia Yang contributed equally to this work.*

† **Electronic supplementary information (ESI) available**: additional experimental results.

1. R. Weissleder and M. J. Pittet, *Nature*, 2008, **452**, 580-589.
2. H. Kobayashi, M. Ogawa, R. Alford, P. L. Choyke and Y. Urano, *Chem. Rev.*, 2009, **110**, 2620-2640.
3. H. Yang, S. Santra, G. A. Walter and P. H. Holloway, *Adv. Mater.*, 2006, **18**, 2890-2894.
4. J. Gao, G. Liang, J. S. Cheung, Y. Pan, Y. Kuang, F. Zhao, B. Zhang, X. Zhang, E. X. Wu and B. Xu, *J. Am. Chem. Soc.*, 2008, **130**, 11828-11833.
5. J. Li, L. Zheng, H. Cai, W. Sun, M. Shen, G. Zhang and X. Shi, *Biomaterials*, 2013, **34**, 8382-8392.
6. J. Li, Y. He, W. Sun, Y. Luo, H. Cai, Y. Pan, M. Shen, J. Xia and X. Shi, *Biomaterials*, 2014, **35**, 3666-3677.
7. S. D. Swanson, J. F. Kukowska-Latallo, A. K. Patri, C. Chen, S. Ge, Z. Cao, A. Kotlyar, A. T. East and J. R. Baker, *Int. J. Nanomed.*, 2008, **3**, 201.
8. R. Popovtzer, A. Agrawal, N. A. Kotov, A. Popovtzer, J. Balter, T. E. Carey and R. Kopelman, *Nano Lett.*, 2008, **8**, 4593-4596.
9. D. Kim, Y. Y. Jeong and S. Jon, *ACS Nano*, 2010, **4**, 3689-3696.
10. C. Alric, J. Taleb, G. L. Duc, C. Mandon, C. Billotey, A. L. Meur-Herland, T. Brochard, F. Vocanson, M. Janier and P. Perriat, *J. Am. Chem. Soc.*, 2008, **130**, 5908-5915.
11. W. Cai and X. Chen, *Small*, 2007, **3**, 1840-1854.
12. H. Wu, H. Shi, H. Zhang, X. Wang, Y. Yang, C. Yu, C. Hao, J. Du, H. Hu and S. Yang, *Biomaterials*, 2014, **35**, 5369-5380.
13. L. An, H. Hu, J. Du, J. Wei, L. Wang, H. Yang, D. Wu, H. Shi, F. Li and S. Yang, *Biomaterials*, 2014, **35**, 5381-5392.
14. J. Cheon and J.-H. Lee, *Accounts Chem. Res.*, 2008, **41**, 1630-1640.
15. K. Tanaka, E. R. O. Siwu, K. Minami, K. Hasegawa, S. Nozaki, Y. Kanayama, K. Koyama, W. C. Chen, J. C. Paulson and Y. Watanabe, *Angew. Chem., Int. Ed.*, 2010, **49**, 8195-8200.
16. D.-E. Lee, H. Koo, I.-C. Sun, J. H. Ryu, K. Kim and I. C. Kwon, *Chem. Soc. Rev.*, 2012, **41**, 2656-2672.
17. V. Biju, *Chem. Soc. Rev.*, 2014, **43**, 744-764.
18. V. Kattumuri, K. Katti, S. Bhaskaran, E. J. Boote, S. W. Casteel, G. M. Fent, D. J. Robertson, M. Chandrasekhar, R. Kannan and K. V. Katti, *Small*, 2007, **3**, 333-341.
19. P. Huang, L. Bao, C. Zhang, J. Lin, T. Luo, D. Yang, M. He, Z. Li, G. Gao and B. Gao, *Biomaterials*, 2011, **32**, 9796-9809.
20. M. Zhou, R. Zhang, M. Huang, W. Lu, S. Song, M. P. Melancon, M. Tian, D. Liang and C. Li, *J. Am. Chem. Soc.*, 2010, **132**, 15351-15358.
21. Y. Jin, J. Wang, H. Ke, S. Wang and Z. Dai, *Biomaterials*, 2013, **34**, 4794-4802.
22. X. Shi, S. H. Wang, S. D. Swanson, S. Ge, Z. Cao, M. E. Van Antwerp, K. J. Landmark and J. R. Baker, *Adv. Mater.*, 2008, **20**, 1671-1678.
23. H. Yang, Y. Zhuang, Y. Sun, A. Dai, X. Shi, D. Wu, F. Li, H. Hu and S. Yang, *Biomaterials*, 2011, **32**, 4584-4593.
24. X. Ji, R. Shao, A. M. Elliott, R. J. Stafford, E. Esparza-Coss, J. A. Bankson, G. Liang, Z.-P. Luo, K. Park and J. T. Markert, *J. Phys. Chem. C*, 2007, **111**, 6245-6251.
25. W. Dong, Y. Li, D. Niu, Z. Ma, J. Gu, Y. Chen, W. Zhao, X. Liu, C. Liu and J. Shi, *Adv. Mater.*, 2011, **23**, 5392-5397.
26. J. Xie, K. Chen, H.-Y. Lee, C. Xu, A. R. Hsu, S. Peng, X. Chen and S. Sun, *J. Am. Chem. Soc.*, 2008, **130**, 7542-7543.
27. Y.-G. Zhai, W.-J. Dong, Y.-P. Gao, D.-C. Niu, J.-Z. Chen, J.-L. Gu, Y.-S. Li and J.-L. Shi, *J. Inorg. Mater.*, 2015, **30**, 950-956.
28. H. Liu, H. Wang, Y. Xu, R. Guo, S. Wen, Y. Huang, W. Liu, M. Shen, J. Zhao and G. Zhang, *ACS Appl. Mater. Interfaces*, 2014, **6**, 6944-6953.
29. Y. Cao, Y. He, H. Liu, Y. Luo, M. Shen, J. Xia and X. Shi, *J. Mater. Chem. B*, 2015, **3**, 286-295.
30. W. Dong, Y. Li, D. Niu, Z. Ma, X. Liu, J. Gu, W. Zhao, Y. Zheng and J. Shi, *Small*, 2013, **9**, 2500-2508.
31. Y. Hu, J. Li, M. Shen and X. Shi, *Chin. Phys. B*, 2014, **23**, 78704-78711.
32. H. Yu, M. Chen, P. M. Rice, S. X. Wang, R. L. White and S. H. Sun, *Nano Lett.*, 2005, **5**, 379-382.
33. J. Bao, W. Chen, T. T. Liu, Y. L. Zhu, P. Y. Jin, L. Y. Wang, J. F. Liu, Y. G. Wei and Y. D. Li, *ACS Nano*, 2007, **1**, 293-298.
34. D. Caruntu, B. L. Cushing, G. Caruntu and C. J. O'Connor, *Chem. Mater.*, 2005, **17**, 3398-3402.
35. H. Cai, K. Li, M. Shen, S. Wen, Y. Luo, C. Peng, G. Zhang and X. Shi, *J. Mater. Chem.*, 2012, **22**, 15110-15120.
36. J. Li, L. Zheng, H. Cai, W. Sun, M. Shen, G. Zhang and X. Shi, *ACS Appl. Mater. Interfaces*, 2013, **5**, 10357-10366.
37. H. Cai, X. An, J. Cui, J. Li, S. Wen, K. Li, M. Shen, L. Zheng, G. Zhang and X. Shi, *ACS Appl. Mater. Interfaces*, 2013, **5**, 1722-1731.
38. J. Zhu, L. Zheng, S. Wen, Y. Tang, M. Shen, G. Zhang and X. Shi, *Biomaterials*, 2014, **35**, 7635-7646.
39. Y. Liu, K. Li, J. Pan, B. Liu and S.-S. Feng, *Biomaterials*, 2010, **31**, 330-338.

40. J.-J. Lin, J.-S. Chen, S.-J. Huang, J.-H. Ko, Y.-M. Wang, T.-L. Chen and L.-F. Wang, *Biomaterials*, 2009, **30**, 5114-5124.
41. D. Pan, J. L. Turner and K. L. Wooley, *Chem. Commun.*, 2003, 2400-2401.
42. H. Yang, C. Qin, C. Yu, Y. Lu, H. Zhang, F. Xue, D. Wu, Z. Zhou and S. Yang, *Adv. Funct. Mater.*, 2014, **24**, 1738-1747.
43. Y. Hu, J. Li, J. Yang, P. Wei, Y. Luo, L. Ding, W. Sun, G. Zhang, X. Shi and M. Shen, *Biomater. Sci.*, 2015, **3**, 721-732.
44. D.-E. Lee, A. Y. Kim, G. Saravanakumar, H. Koo, I. C. Kwon, K. Choi, J. H. Park and K. Kim, *Macromol. Res.*, 2011, **19**, 861-867.
45. J. Li, Y. Hu, J. Yang, P. Wei, W. Sun, M. Shen, G. Zhang and X. Shi, *Biomaterials*, 2015, **38**, 10-21.
46. M. H. El-Dakdouki, K. El-Boubbou, M. Kamat, R. Huang, G. S. Abela, M. Kiupel, D. C. Zhu and X. Huang, *Pharm. Res.*, 2013, **31**, 1426-1437.
47. X. Shi, S. Wang, S. Meshinchi, M. E. Van Antwerp, X. Bi, I. Lee and J. R. Baker, *Small*, 2007, **3**, 1245-1252.
48. C. Wang, S. Wang, K. Li, Y. Ju, J. Li, Y. Zhang, J. Li, X. Liu, X. Shi and Q. Zhao, *PloS one*, 2014, **9**, e99585.
49. M. Ma, H. Chen, Y. Chen, K. Zhang, X. Wang, X. Cui and J. Shi, *J. Mater. Chem.*, 2012, **22**, 5615-5621.
50. F. Li, S.-J. Park, D. Ling, W. Park, J. Y. Han, K. Na and K. Char, *J. Mater. Chem. B*, 2013, **1**, 1678-1686.
51. B. Zhou, L. Zheng, C. Peng, D. Li, J. Li, S. Wen, M. Shen, G. Zhang and X. Shi, *ACS Appl. Mater. Interfaces*, 2014, **6**, 17190-17199.
52. S. Arpicco, C. Lerda, E. D. Pozza, C. Costanzo, N. Tsapis, B. Stella, M. Donadelli, I. Dando, E. Fattal, L. Cattel and M. Palmieri, *Eur. J. Pharm. Biopharm.*, 2013, **85**, 373-380.
53. S. Magnitsky, D. J. Watson, R. M. Walton, S. Pickup, J. W. M. Bulte, J. H. Wolfe and H. Poptani, *Neuroimage*, 2005, **26**, 744-754.
54. J.-W. Yoo, E. Chambers and S. Mitragotri, *Curr. Pharm. Design*, 2010, **16**, 2298-2307.
55. H. Hu, A. Dai, J. Sun, X. Li, F. Gao, L. Wu, Y. Fang, H. Yang, L. An and H. Wu, *Nanoscale*, 2013, **5**, 10447-10454.

Table 1. Zeta potential, hydrodynamic size, and polydispersity index of the Fe_3O_4/Au-PEI and Fe_3O_4/Au-PEI-HA CNPs. Data are provided as mean ± S.D. (n= 3)

Materials	Zeta potential (mV)	Hydrodynamic size (nm)	Polydispersity index (PDI)
Fe_3O_4/Au-PEI	+36.1 ± 1.1	339.3 ± 4.3	0.31 ± 0.02
Fe_3O_4/Au-PEI-HA	−19.6 ± 1.6	384.2 ± 3.2	0.28 ± 0.02

Figure captions

Scheme 1. Schematic representation of the synthesis of the Fe_3O_4/Au-PEI-HA CNPs.

Fig. 1. (a) UV-vis spectra of the Fe_3O_4-PEI NPs and the Fe_3O_4/Au-PEI CNPs; (b) XRD pattern of the Fe_3O_4/Au-PEI CNPs.

Fig. 2. TEM image (a) and EDS spectrum (b) of the Fe_3O_4/Au-PEI-HA CNPs. Inset of (a) shows the enlarged TEM image of the CNPs.

Fig. 3. (a) T_2-weighted MR images of the Fe_3O_4/Au-PEI-HA CNPs (a) with different Fe concentrations (0.0025, 0.005, 0.01, and 0.02 mM, respectively); (b) linear fitting of $1/T_2$ of the CNPs as a function of Fe concentration; (c) CT images of the Fe_3O_4/Au-PEI-HA CNPs with different Au concentrations (2, 4, 8, and 16 mM, respectively); (d) linear fitting of the CT value (HU) of the CNPs as a function of Au concentration.

Fig. 4. Hemolytical activity of the Fe_3O_4/Au-PEI-HA CNPs at different Fe concentrations (50, 100, 300, and 600 μg/mL, respectively). PBS and water were used as negative and positive control, respectively. The bottom-right inset shows the photograph of HRBCs exposed to water, PBS, and PBS containing the CNPs at different Fe concentrations for 2 h, followed by centrifugation. The upper-right inset shows the enlarged UV-vis spectra indicated by the arrow.

Fig. 5. MTT viability assay of HeLa cells after treated with the Fe_3O_4/Au-PEI-HA CNPs in an Fe concentration range of 0.2-2.0 mM for 24 h. Data are represented as mean ± S.D. (n =3).

Fig. 6. Uptake of Fe in HeLa-LCD44 or HeLa-HCD44 cells treated with the Fe_3O_4/Au-PEI-HA CNPs with different Fe concentrations (0.2, 0.4, and 0.6 mM, respectively) for 4 h. HeLa cells treated with PBS were used as control.

Fig. 7. Phase contrast microscopic images of the Prussian blue-stained HeLa-LCD44 cells (a-d) and HeLa-HCD44 cells (e-h) after treated with PBS (as a control) and the Fe_3O_4/Au-PEI-HA CNPs at an

Fe concentration of 0.2 (b, f), 0.4 (c, g), and 0.6 (d, h) mM, respectively for 4 h.

Fig. 8. T_2-weighted MR images (a) and MR signal intensity (b) of the HeLa-LCD44 or HeLa-HCD44 cells incubated with the Fe_3O_4/Au-PEI-HA CNPs at different Fe concentrations (0.1, 0.2, 0.4, and 0.6 mM, respectively) for 6 h. CT images (c) and CT value (d) of both cells incubated with the particles at different Au concentrations (0.125, 0.25, 0.5, and 1.0 mM, respectively) for 6 h. In (a) and (c), 1 and 2 represent the HeLa-LCD44 and HeLa-HCD44 cells, respectively.

Fig. 9. Time-dependent *in vivo* T_2-weighted MR images (a), MR signal intensity (b), CT images (c), and CT value (d) of tumors after the mice were intravenously injected with the Fe_3O_4/Au-PEI-HA CNPs ([Fe] = 215.29 mM, [Au] = 50 mM, 0.1 mL PBS) (Group 1, injected with the Fe_3O_4/Au-PEI-HA CNPs; Group 2, pre-treated with free HA (1 mM, 0.1 mL) for 1 h and then injected with the Fe_3O_4/Au-PEI-HA CNPs; and Group 3, injected with the mixture of free HA (1 mM) and the Fe_3O_4/Au-PEI-HA CNPs).

Fig. 10. H&E stained tissue sections of mice at 15 days postinjection of the Fe_3O_4/Au-PEI-HA CNPs ([Fe] = 215.29 mM, [Au] = 50 mM, 0.1 mL PBS). The mice treated with PBS were used as control. The scale bars in each panel represent 100 μm.

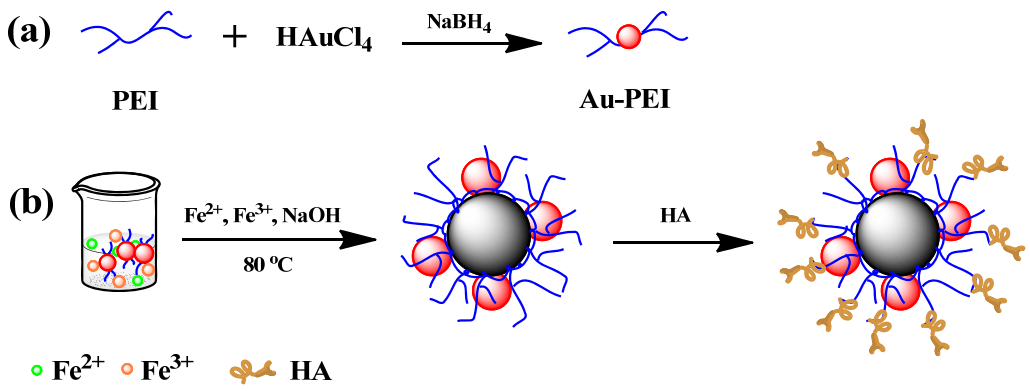

Scheme 1

Hu *et al*.

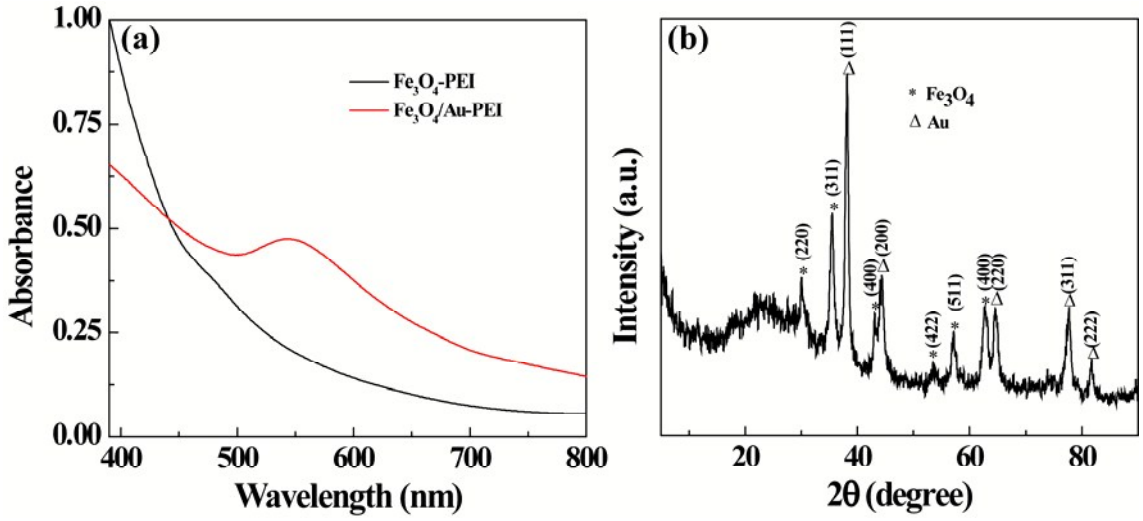

Fig. 1

Hu *et al*.

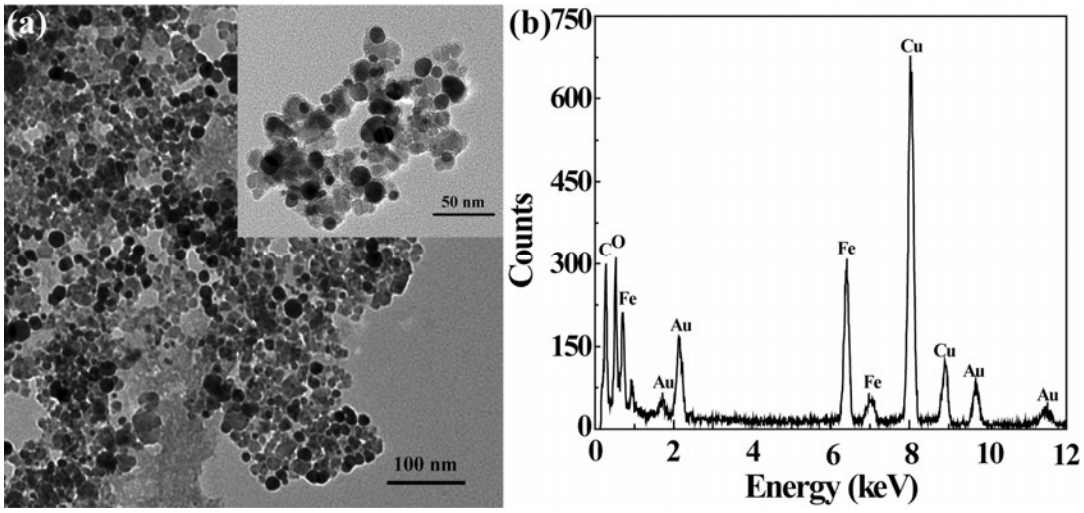

Fig. 2

Hu *et al*.

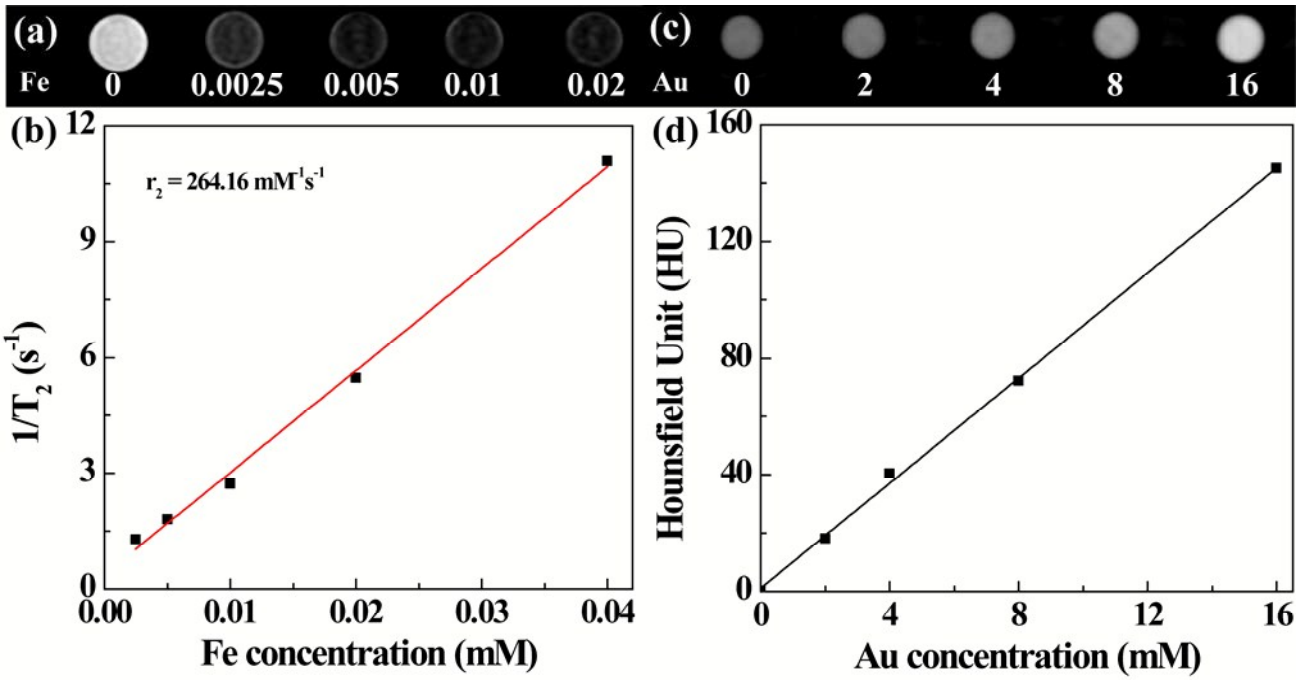

Fig. 3

Hu *et al*.

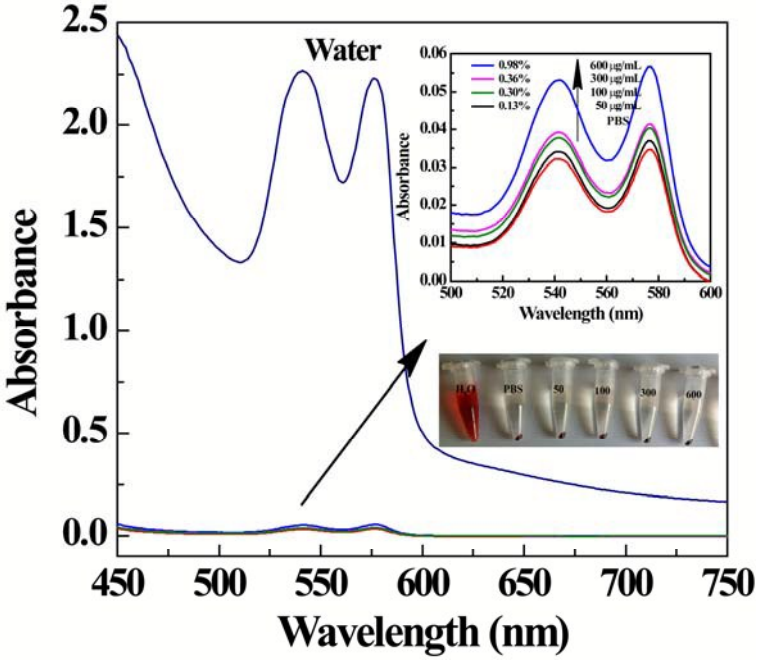

Fig. 4

Hu *et al*.

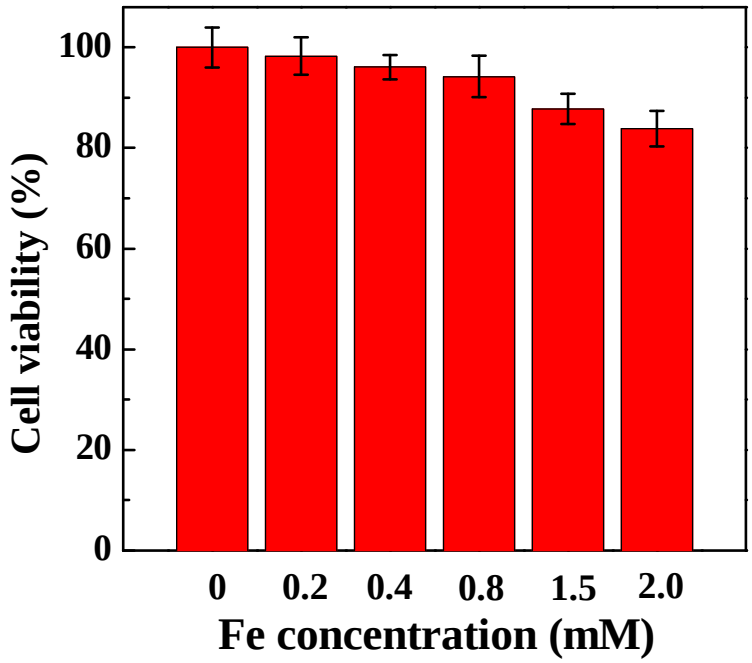

Fig. 5

Hu *et al*.

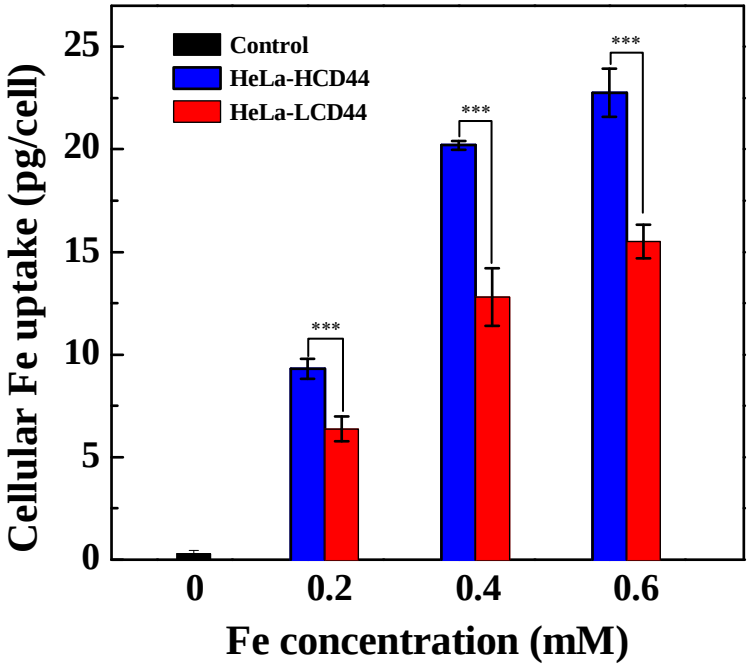

Fig. 6

Hu *et al*.

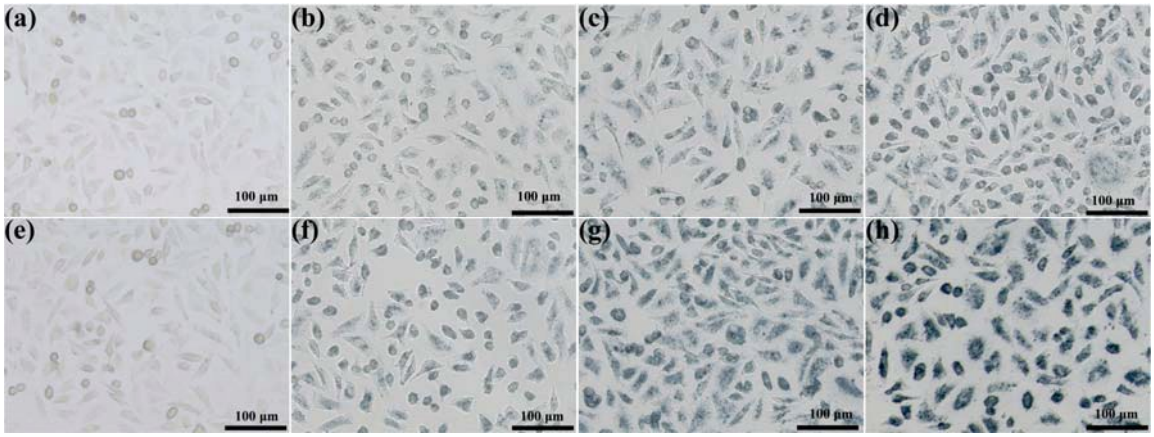

Fig. 7

Hu *et al*.

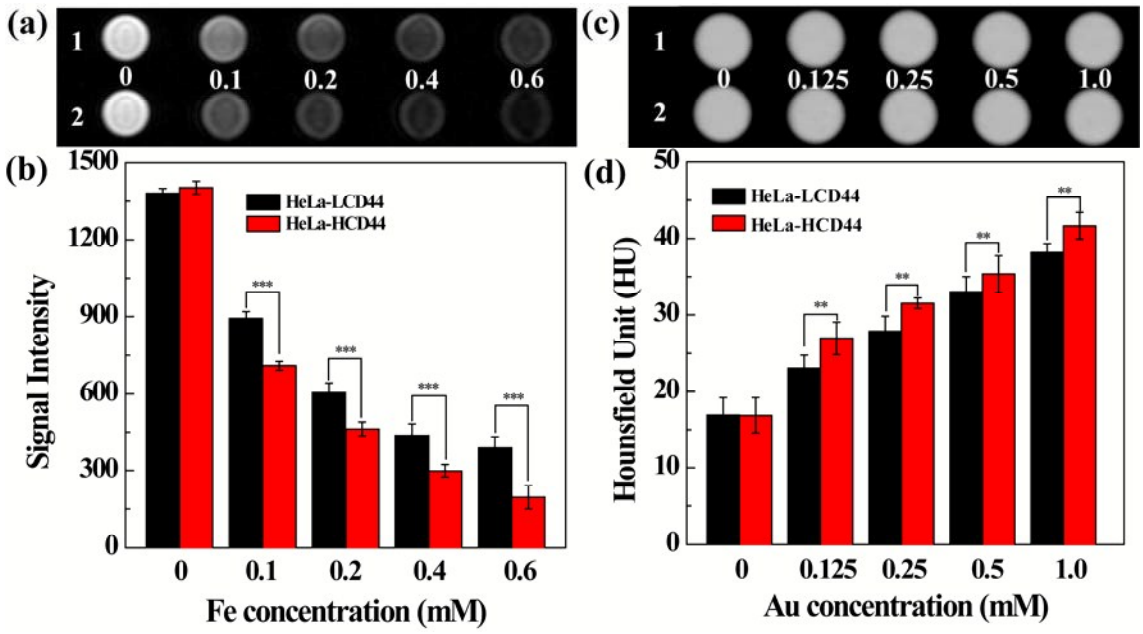

Fig. 8

Hu *et al.*

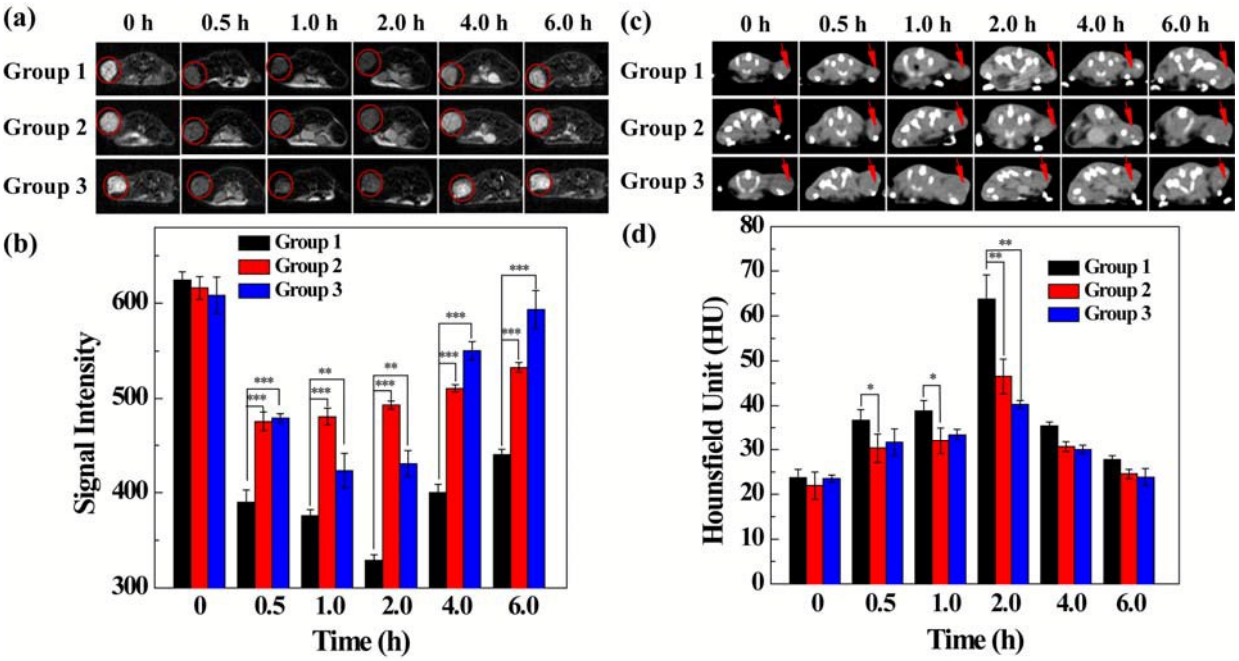

Fig. 9

Hu *et al.*

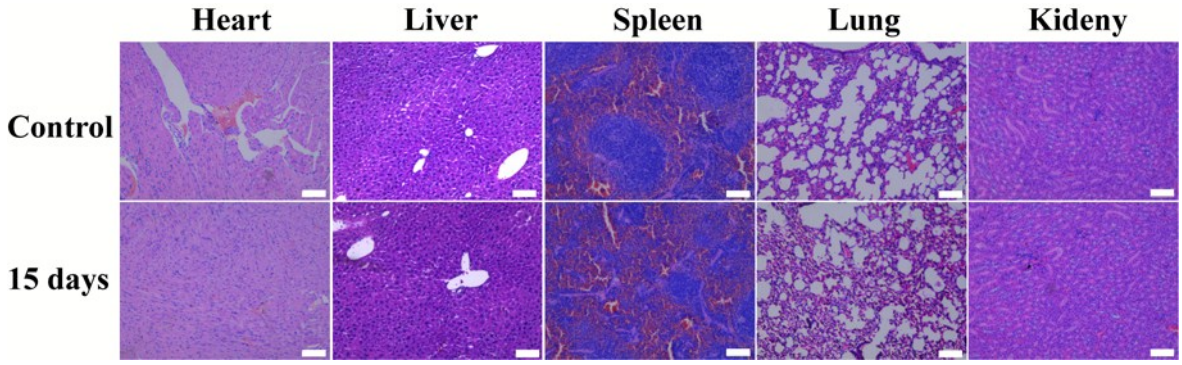

Fig. 10

Hu *et al.*

Table of Contents (TOC)

Facile synthesis of hyaluronic acid-modified Fe_3O_4/Au composite nanoparticles for targeted dual mode MR/CT imaging of tumors†

Yong Hu,[a1] Jia Yang,[b1] Ping Wei,[a] Jingchao Li,[a] Ling Ding,[a] Guixiang Zhang,[b]* Xiangyang Shi,[a]* Mingwu Shen[a]*

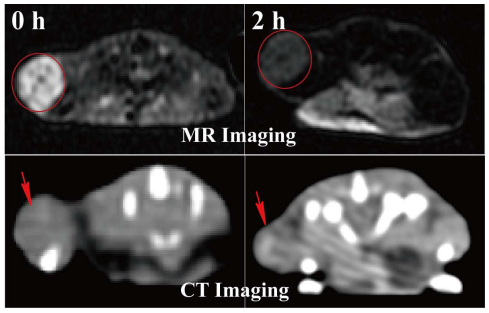

Hyaluronic acid-modified Fe_3O_4/Au composite nanoparticles can be synthesized for targeted dual mode MR/CT imaging of tumors.